Debonding Detection in Carbon Fiber Reinforced Polymer Plate Repaired Steel Beam Using Percussion and Gaussian Mixture Model Clustering

Yong Xu
Dept. of Mech. Eng.
University of Houston
Houston, USA
yxu23@uh.edu

Ji-An Chen
Dept. of Mech. Eng.
University of Houston
Houston, USA
jchen216@cougarnet.uh.edu

Xuemin Chen
Dept. of Engineering
Texas Southern University
Houston, USA
xuemin.chen@tsu.edu

Gangbing Song
Dept. of Mech. Eng.
University of Houston
Houston, USA
gsong@uh.edu

***Abstract*—The carbon fiber reinforced polymer (CFRP) has been proven to be a cost-effective, efficient, and reliable method for structural rehabilitation or reinforcement. Debonding detection is an important measure to ensure the integrity and performance of such repairs. In this paper, a method of using percussion and unsupervised machine learning to detect the debonding of CFRP plate repaired steel structure is proposed. A steel beam with bonded CFRP and known bonding defects is used as a test specimen. Then, different locations with different bonding conditions on the beam are tapped to generate the percussion sounds, which are recorded by an iPhone. The mel-frequency cepstral coefficient (MFCC) algorithm is employed to extract features from percussion sounds. The unsupervised machine learning algorithm, Gaussian mixture model (GMM) clustering, is implemented for debonding detection. The proposed method achieves 95.8% accuracy in debonding detection on the test specimen.**

***Index Terms*—percussion, Gaussian mixture model, mel-frequency cepstral coefficient, carbon fiber reinforced polymer, unsupervised machine learning**

I. Introduction

Civil infrastructures are prone to damages due to a variety of adverse effects, such as vibration [1] [2], impact [3] [4], corrosion [5] [6], and temperate cycling [7]. The collapse of Pittsburgh's Fern Hollow Bridge in Pennsylvania brings attention to the structurally deficient bridges. The carbon fiber reinforced polymer (CFRP) has been proven to be a cost-effective, efficient, and reliable method for steel structural rehabilitation [8] [9]. The debonding is one of the main failure modes of the CFRP repaired steel structure [10] [11]. Benefited from the recent rapid development in structural health monitoring (SHM) [12]–[15], the current methods applied to detecting the debonding include the piezoceramic transducer based methods [16]–[18], ultrasonics [19] [20] and X-ray based methods [21] [22]. However, these methods require installation of sensors or using complex instruments. Therefore they are not convenient in field applications.

A new trend in structural health monitoring has been developed is the percussion method. This method uses the tapping and listening to collect data, then uses machine learning to interpret the data. Many factors will affect structural acoustic response when the structure is subject to percussion or excitation [23]–[25]. Recently, numerous successful percussion-based applications have been reported for the bolt looseness monitoring [26]–[29], concrete moisture level monitoring [30], concrete-filled steel tubular voids detection [31] [32], pipeline sand deposition detection [33], cup-lock scaffolds looseness detection [34], and through bolts shear loading detection [35]. The percussion method is receiving increasing attention due to the advantage that it does not require the installation of sensors or using complex equipment. In addition, the recent development in machine learning such as neural network provides effective interpretation of relationship between the percussion-induced sounds and the structural properties [23]–[25].

In this paper, the percussion method is applied to the debonding detection in CFRP plate repaired steel-beam, and the Gaussian mixture model (GMM) clustering is implemented to interpret the percussion-induced sounds. A specimen is designed and fabricated to facilitate the investigation, and percussion data are collected on the specimen. Experimental results are analyzed for verification of effectiveness of the proposed method.

II. The Proposed Method

The percussion sound is processed to generate the mel-frequency cepstral coefficient (MFCC). The mean and standard deviation are calculated for each MFCC and served as source of the feature data. The features are manually selected and formed as sample data for GMM clustering.

A. MFCC

The MFCC is an audio signal process method. It uses Hamming window to partition the sound data, and then the discrete Fourier transformation (DFT) is applied to the windowed data. After that, the data processed by DFT go through the Mel filter bank. The discrete cosine transform (DCT) is employed at last

This material was based upon work partially supported by the National Science Foundation under Grant No. 1801811.

978-1-6654-9835-7/22/$31.00 ©2022 IEEE

to calculate the coefficient. Specific steps for the process are as follows [36].

Let $x(n)$ represent the audio data and $s(n)$ designate the data processed by respective Hamming window function $w(n)$ [37], and $s(n)$ is

$$s(n) = x(n)w(n), 0 \leqslant n \leqslant L-1, \tag{1}$$

where

$$w(n) = 0.54 - 0.46\cos(2\pi\frac{n}{L-1}), \tag{2}$$

L is the window length. The $s(n)$ of each window is then processed by DFT,

$$S(j) = \sum_{n=0}^{L-1} s(n)e^{-\frac{i2\pi}{L}nj}, 0 \leqslant j \leqslant L-1. \tag{3}$$

The data then pass through the Mel filter bank $H_m(j)$ to generate the Mel spectrum $t(m)$,

$$t(m) = \sum_{j=0}^{L-1}\left[|S(j)|^2 H_m(j)\right], 0 \leqslant m \leqslant M-1, \tag{4}$$

where M is number of Mel filters,

$$H_m(j) = \begin{cases} 0, & j < f(m-1) \\ \frac{2(j-f(m-1))}{f(m)-f(m-1)}, & f(m-1) \leqslant j \leqslant f(m) \\ \frac{2(f(m+1)-j)}{f(m+1)-f(m)}, & f(m) \leqslant j \leqslant f(m+1) \\ 0, & j > f(m+1) \end{cases} \tag{5}$$

Finally, the cepstral coefficients are calculated as

$$c(k) = \sum_{m=0}^{M-1} \log_{10}(t(m))\cos(\frac{\pi k(m-0.5)}{M}). \tag{6}$$

B. GMM

A GMM is a probability density function which is sum of Gaussian component densities. Each Gaussian component is a Gaussian distribution with its own weight for the GMM [38] [39]. A GMM with M components is given by [38]

$$p(x|\lambda) = \sum_{i=1}^{M} w_i g(x|\mu_i, \Sigma_i), \tag{7}$$

where x is the sample data, w_i are the mixture weights, and $g(x|\mu_i, \Sigma_i)$ are the component Gaussian densities.

$$g(x|\mu_i, \Sigma_i) = \frac{exp(-\frac{1}{2}(x-\mu_i)^{'}\Sigma_i^{-1}(x-\mu_i))}{(2\pi)^{\frac{D}{2}}|\Sigma_i|^{\frac{1}{2}}}, \tag{8}$$

where D is dimension of sample data, Σ_i is covariance matrix and μ_i is mean vector.

The GMM model uses the expectation-maximization (EM) algorithm to fit the model. In the expectation step, the posterior probability $P_r(i|x_t, \lambda)$ of a data point x_t for each Gaussian component is calculated [38]

$$P_r(i|x_t, \lambda) = \frac{w_i g(x_t|\mu_i, \Sigma_i)}{\sum_{k=1}^{M} w_k g(x_t|\mu_k, \Sigma_k)}. \tag{9}$$

Next, in the maximization step, the mean vector $\overline{\mu}_i$, covariance matrices $\overline{\Sigma}_i$ and mixture weights $\overline{w}_i$ are updated for each Gaussian component, increasing the model's likelihood value [38].

$$\overline{w}_i = \frac{1}{T}\sum_{t=1}^{T} P_r(i|x_t, \lambda), \tag{10}$$

$$\overline{\mu}_i = \frac{\sum_{t=1}^{T} P_r(i|x_t, \lambda)x_t}{\sum_{t=1}^{T} P_r(i|x_t, \lambda)}, \tag{11}$$

$$\overline{\Sigma}_i = \frac{\sum_{t=1}^{T} P_r(i|x_t, \lambda)(x_t - \overline{\mu}_i)(x_t - \overline{\mu}_i)^{'}}{\sum_{t=1}^{T} P_r(i|x_t, \lambda)}. \tag{12}$$

The EM process iterates until the model converge and then the model compares posterior probability of each data between every Gaussian component. The data point is assigned to the Gaussian component with the highest posterior probability, so finally data are clustered on each Gaussian component.

C. Experiment

The test specimen is an I-shape steel beam with the CFRP plate bonded on the top, as shown in Fig. 1. The voids are created in adhesive to simulate the debonding defects. The surface of the CFRP plate is marked as grids. There are three classes, the healthy grid, which means no void below the CFRP plate; the half-healthy grid, which means there is partial void below the plate; and the unhealthy grid, which means complete void below the plate. Fig. 2 depicts the mapping of grids. The blank cells are healthy grids; the cell with red X are unhealthy grids, and cells with orange color patterns are half-healthy grids.

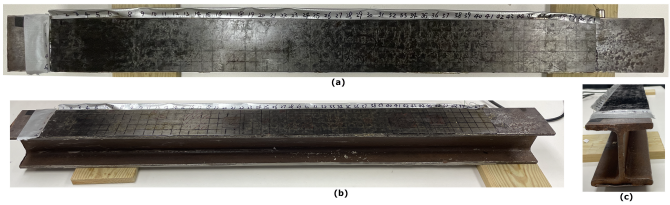

Fig. 1. Steel beam specimen (a) top view (b) front view (c) side view.

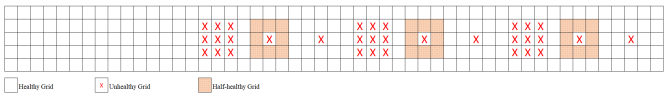

Fig. 2. Mapping of grids shows location of different sample classes, empty cell is healthy grid, cell with orange color pattern is half-healthy grid, cell with red X is unhealthy grid.

During the experiment, a steel bar is used to tap the sample grid. Each grid is hit 7 times as shown in Fig. 3. In total, there are 1085 hits on healthy grids, 189 hits on unhealthy grids and 140 hits on half-healthy grids. Table I summarizes the number of percussion sounds collected on the test specimen.

The percussion sound is recorded by an iPhone. Then the audio files are exported to the computer, and split into many

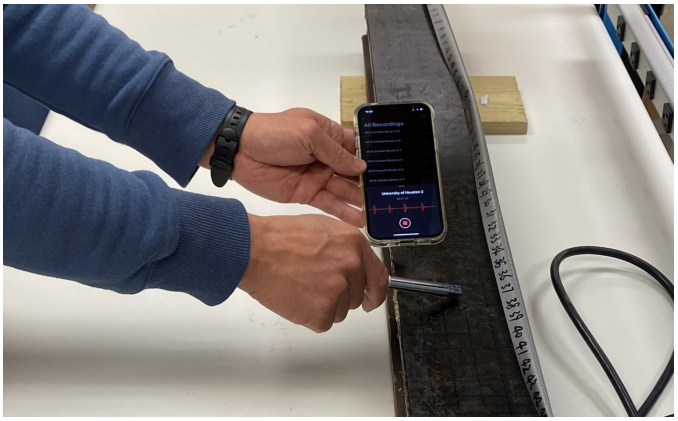

Fig. 3. Percussion sound recording by iPhone.

TABLE I
NUMBER OF SAMPLE HITS ON THE TEST SPECIMEN

Class	Number of Grids	Hits per Grid	Total Sample Hits
Healthy	155	7	1085
Half-healthy	20	7	140
Unhealthy	27	7	189

single hit audios. The MFCC is extracted from the each hit audio signal. In this test, 13 MFCCs are used, which is identified as MFCC 2 to MFCC 14 hereafter, each one is a column in MFCC matrix. The first column MFCC 1 is log energy of the audio signal. To select the feature data for GMM, the MFCC are transformed to a row vector. The mean and standard deviation of each kind of coefficient are calculated. The boxplot of the mean and standard deviation of the MFCC is used for feature selection. Fig. 4 displays boxplot of the mean of MFCC, Fig. 5 displays the box plot of standard deviation of MFCC. From the boxplot, the mean of MFCC 4 provides good differentiation between healthy and other classes samples; mean of MFCC 5 well differentiates healthy and half-healthy samples; mean of MFCC 6 differentiates half-healthy versus other classes samples. They constitutes the feature data set 1. Additional feature sets are selected by adding mean of MFCC 9 which differentiates healthy versus other classes, standard deviation of MFCC 4, which differentiates healthy and unhealthy classes and standard deviation of MFCC 6 which differentiates half-healthy and other classes. The selected feature sets are listed in Table II.

TABLE II
FEATURE SETS FOR GMM

Set Number	Features
Feature Set 1	Mean (MFCC 4, 5, 6)
Feature Set 2	Mean (MFCC 5, 6), STD (MFCC 4)
Feature Set 3	Mean (MFCC 4, 5), STD (MFCC 6)
Feature Set 4	Mean (MFCC 4, 5, 6), STD (MFCC 4, 6)
Feature Set 5	Mean (MFCC 4, 5, 6, 9)

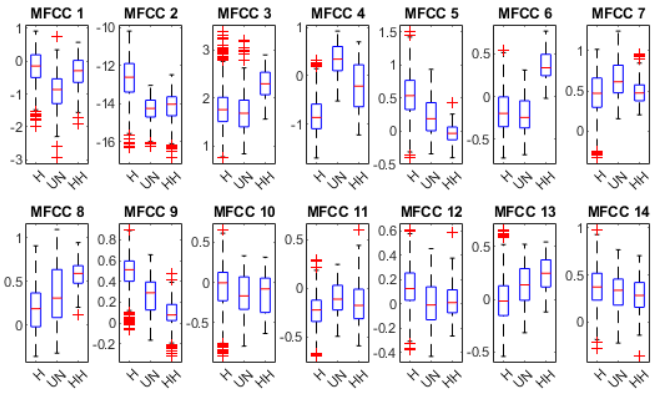

Fig. 4. Mean of MFCC, x axis is health classes, H (Healthy) UN (Unhealthy) HH (Half-healthy).

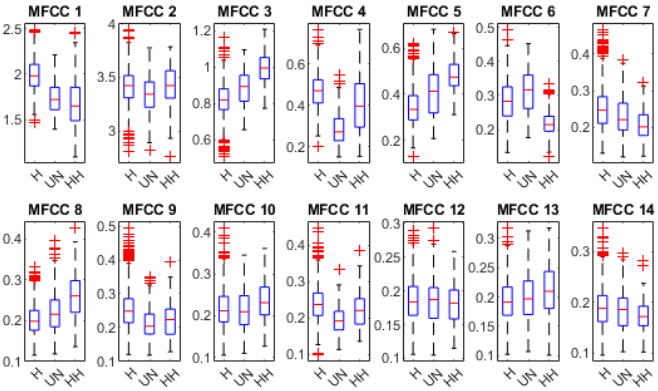

Fig. 5. Standard Deviation of MFCC, x axis is health classes, H (Healthy) UN (Unhealthy) HH (Half-healthy).

III. EXPERIMENTAL RESULTS AND DISCUSSION

The GMM clustering is conducted 10 times for each feature set listed in Table II. Fig. 6 shows the clustering accuracy of every test number for each feature set.

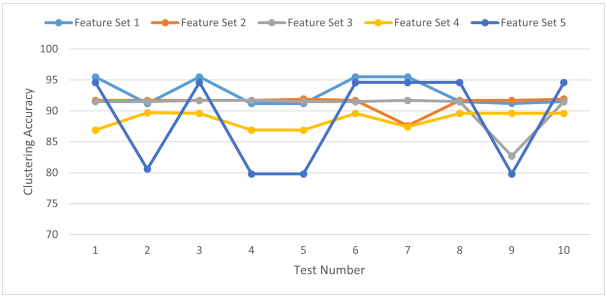

Fig. 6. GMM Clustering Accuracy of Different Feature Set

The feature set 1 which consists of mean of MFCC 4, MFCC 5, and MFCC 6 has the highest average clustering accuracy. It also has the highest clustering accuracy of 95.8%. The results of different feature sets show that the feature which can well differentiate the classes will achieve higher clustering

accuracy. The feature set 1 has the highest clustering accuracy, because the mean of MFCC 4 well differentiates healthy and unhealthy classes, mean of MFCC 5 well differentiates healthy and half-healthy classes, and mean of MFCC 6 well differentiates half-healthy and other classes, as shown in Fig. 4. For feature set 2, the mean of MFCC 4 is replaced by the standard deviation of MFCC 4, which also differentiates healthy and unhealthy classes as shown in Fig. 5, though difference margin is less compare with the mean of MFCC 4. Hence the clustering accuracy of the feature set 2 is lower, which is between 87.6% to 91.9%. Similarly, in feature set 3, the mean of MFCC 6 is replaced by standard deviation of MFCC 6, which differentiates healthy and half-healthy classes, but the difference margin is less compared with the mean of MFCC 6. So the clustering accuracy of feature set 3 is also lower. The accuracy is between 82.7% to 91.7%.

The results indicate that adding more features does not necessary increase the clustering accuracy. The feature set 4 contains 5 features, which adds the standard deviation of MFCC 4 and MFCC 6 into feature set 1. The clustering accuracy is between 86.9% to 89.7%. The feature set 5 adds mean of MFCC 9 into the feature set 1. The clustering accuracy is between 79.8% to 94.6%. Overall, the manual inspection of the boxplot of the mean and standard deviation of MFCC is a feasible method of feature selection for GMM clustering. Though the manual feature selection requires lot of effort and the result is subjective. Future study can be investigated to develop the algorithm to evaluate and select feature data automatically.

Fig. 7 depicts the confusion matrix of the GMM clustering of feature set 1 for the test with 95.8% clustering accuracy. The target class indicates the actual class of the sample data. The output class is the clustering results, which may deviate from the actual class. The green diagonal cells summarize the sample data which are clustered correctly. So output class is same as the target class. The red off diagonal cells are sample data clustered incorrectly. The confusion matrix shows that the half-healthy class is the most challenge one to be clustered correctly. The accuracy is 77.3% only. This is partly because of the variance of hitting point on the half-healthy grid. The hitting point is not always on the boundary between healthy and unhealthy area. When the hitting point is close to healthy area, the percussion sound is more similar to the sound from the healthy area. On the other hand, when the hitting point is close to the unhealthy area, then sound is more similar to unhealthy class.

In this experiment, the sample data are highly unbalanced, 77% of the percussion-induced data are in healthy class, 13% of data are in unhealthy class, and only 10% of data are in half-healthy class. The result demonstrates that GMM clustering works well with unbalanced data.

IV. Conclusions

The strengthening of steel beam by CFRP plate is a convenient and reliable solution for structural rehabilitation. The performance of the CFRP repaired steel beam is highly

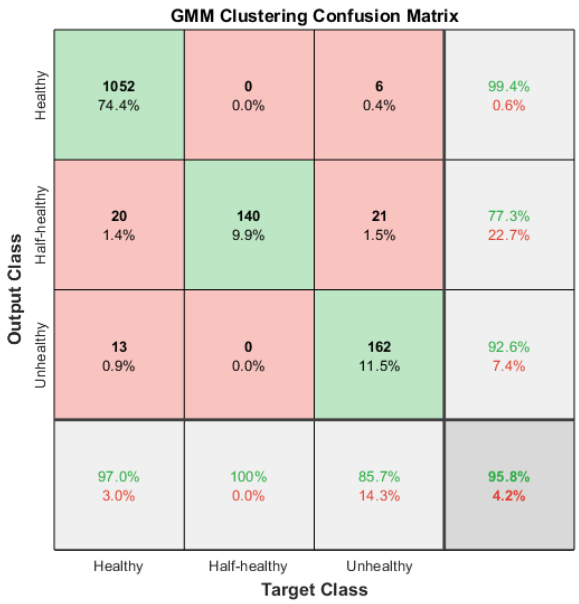

Fig. 7. GMM Clustering Confusion Matrix for Feature Set 1.

dependent on the bonding quality. In this paper, the method of debonding detection in CFRP plate repaired steel beam using percussion and GMM clustering was implemented and validated on the test specimen. The proposed method achieved 95.8% clustering accuracy. The sample data of three classes were clustered successfully. Compared with the conventional method which requires installation of sensors, the proposed method using the percussion and machine learning is more flexible. It does not require installation of sensors or test instruments. The MFCCs are extracted from the audio data, the mean and standard deviation of the MFCCs are used as feature data. The result proves this is an effective feature extraction and transformation method for the percussion sound. The sample data are unbalanced, and the majority of data belong to healthy class. The GMM clustering can handle the unbalanced data well and achieve high accuracy. The proposed method opens a door for future automated debonding detection of CFRP plate repaired structures by using robotics enabled percussion method. In this paper the feature set was manually selected. Future works include developing an automatic feature selection algorithm to address the manual selection of feature sets, and applying the proposed method on actual structure to evaluate its performance in field application.

References

[1] W. Wang, X. Wang, X. Hua, G. Song, and Z. Chen, "Vibration control of vortex-induced vibrations of a bridge deck by a single-side pounding tuned mass damper," *Engineering Structures*, vol. 173, pp. 61–75, 2018.

[2] X. Yin, G. Song, and Y. Liu, "Vibration suppression of wind/traffic/bridge coupled system using multiple pounding tuned mass dampers (MPTMD)," *Sensors*, vol. 19, no. 5, p. 1133, 2019.

[3] G. Song, C. Olmi, and H. Gu, "An overheight vehicle–bridge collision monitoring system using piezoelectric transducers," *Smart Materials and Structures*, vol. 16, no. 2, p. 462, 2007.

[4] Y. Sha and H. Hao, "Numerical simulation of barge impact on a continuous girder bridge and bridge damage detection," *International Journal of Protective Structures*, vol. 4, no. 1, pp. 79–96, 2013.

[5] L. Xiao, J. Peng, J. Zhang, Y. Ma, and C. Cai, "Comparative assessment of mechanical properties of HPS between electrochemical corrosion and spray corrosion," *Construction and Building Materials*, vol. 237, p. 117735, 2020.

[6] L. Huo, C. Li, T. Jiang, and H.-N. Li, "Feasibility study of steel bar corrosion monitoring using a piezoceramic transducer enabled time reversal method," *Applied Sciences*, vol. 8, no. 11, p. 2304, 2018.

[7] A. Mosallam, H. Xin, S. He, A. A. Agwa, S. Adanur, and M. A. Salama, "Thermal cycling and ultraviolet radiation effects on fatigue performance of triaxial CFRP laminates for bridge applications," *Journal of Composite Materials*, vol. 56, no. 2, pp. 279–294, 2022.

[8] A. H. Al-Saidy, F. Klaiber, and T. Wipf, "Repair of steel composite beams with carbon fiber-reinforced polymer plates," *Journal of Composites for Construction*, vol. 8, no. 2, pp. 163–172, 2004.

[9] B. Di, J. Wang, H. Li, J. Zheng, Y. Zheng, and G. Song, "Investigation of bonding behavior of FRP and steel bars in self-compacting concrete structures using acoustic emission method," *Sensors*, vol. 19, no. 1, p. 159, 2019.

[10] Y. Yang, C.-T. Ng, and A. Kotousov, "Second harmonic generation of guided wave at crack-induced debonding in FRP-strengthened metallic plates," *International Journal of Structural Stability and Dynamics*, vol. 19, no. 01, p. 1940006, 2019.

[11] M. Hamrat, F. Bouziadi, B. Boulekbache, T. H. Daouadji, S. Chergui, A. Labed, and S. Amziane, "Experimental and numerical investigation on the deflection behavior of pre-cracked and repaired reinforced concrete beams with fiber-reinforced polymer," *Construction and Building Materials*, vol. 249, p. 118745, 2020.

[12] Q. Kong, S. Hou, Q. Ji, Y. Mo, and G. Song, "Very early age concrete hydration characterization monitoring using piezoceramic based smart aggregates," *Smart Materials and Structures*, vol. 22, no. 8, p. 085025, 2013.

[13] Q. Kong, R. H. Robert, P. Silva, and Y. Mo, "Cyclic crack monitoring of a reinforced concrete column under simulated pseudo-dynamic loading using piezoceramic-based smart aggregates," *Applied Sciences*, vol. 6, no. 11, p. 341, 2016.

[14] G. Loubet, A. Takacs, and D. Dragomirescu, "Implementation of a battery-free wireless sensor for cyber-physical systems dedicated to structural health monitoring applications," *IEEE Access*, vol. 7, pp. 24 679–24 690, 2019.

[15] M. Zhang, X. Chen, and W. Li, "A hybrid hidden Markov model for pipeline leakage detection," *Applied Sciences*, vol. 11, no. 7, 2021. [Online]. Available: https://www.mdpi.com/2076-3417/11/7/3138

[16] T. Jiang, Q. Kong, D. Patil, Z. Luo, L. Huo, and G. Song, "Detection of debonding between fiber reinforced polymer bar and concrete structure using piezoceramic transducers and wavelet packet analysis," *IEEE Sensors Journal*, vol. 17, no. 7, pp. 1992–1998, 2017.

[17] K. Xu, C. Ren, Q. Deng, Q. Jin, and X. Chen, "Real-time monitoring of bond slip between GFRP bar and concrete structure using piezoceramic transducer-enabled active sensing," *Sensors*, vol. 18, no. 8, p. 2653, 2018.

[18] J. Jiang, J. Jiang, X. Deng, and Z. Deng, "Detecting debonding between steel beam and reinforcing CFRP plate using active sensing with removable PZT-based transducers," *Sensors*, vol. 20, no. 1, p. 41, 2020.

[19] L. Huo, H. Cheng, Q. Kong, and X. Chen, "Bond-slip monitoring of concrete structures using smart sensors—a review," *Sensors*, vol. 19, no. 5, p. 1231, 2019.

[20] V. Dattoma, R. Nobile, F. Palano, F. Panella, A. Pirinu, and A. Saponaro, "Ultrasonic and thermographic fatigue monitoring on a full-scale CFRP aeronautical component after repairing," in *IOP Conference Series: Materials Science and Engineering*, vol. 1038, no. 1. IOP Publishing, 2021, p. 012027.

[21] C. E. Wood, N. O'Brien, A. Denysov, and T. Blumensath, "Computed laminography of CFRP using an X-ray cone-beam and robotic sample manipulator systems," *IEEE Transactions on Nuclear Science*, vol. 66, no. 3, pp. 655–663, 2019.

[22] E. Reis and U. Dilek, "Non-destructive radiographic evaluation and repairs to pre-stressed structures following partial collapse," in *Forensic Engineering 2012: Gateway to a Better Tomorrow*, 2013, pp. 1015–1023.

[23] L. Chen, H. Xiong, Z. Yang, Y. Long, Y. Ding, and Q. Kong, "Preload measurement of steel-to-timber bolted joint using piezoceramic-based electromechanical impedance method," *Measurement*, p. 110725, 2022.

[24] Q. Kong, K. Ji, J. Gu, L. Chen, and C. Yuan, "A CNN-integrated percussion method for detection of FRP–concrete interfacial damage with FEM reconstruction," *Structural Health Monitoring*, p. 14759217221082007, 2022.

[25] F. Wang and R. Zhu, "Detection of bolt head corrosion under external vibration using a novel entropy-enhanced acoustic emission method," *Nonlinear Dynamics*, pp. 1–10, 2022.

[26] R. Yuan, Y. Lv, Q. Kong, and G. Song, "Percussion-based bolt looseness monitoring using intrinsic multiscale entropy analysis and BP neural network," *Smart Materials and Structures*, vol. 28, no. 12, p. 125001, 2019.

[27] F. Wang and G. Song, "Bolt-looseness detection by a new percussion-based method using multifractal analysis and gradient boosting decision tree," *Structural Health Monitoring*, vol. 19, no. 6, pp. 2023–2032, 2020.

[28] ——, "A novel percussion-based method for multi-bolt looseness detection using one-dimensional memory augmented convolutional long short-term memory networks," *Mechanical Systems and Signal Processing*, vol. 161, p. 107955, 2021.

[29] F. Wang, X. Chen, and G. Song, "Percussion-based detection of bolt looseness using speech recognition technology and least square support vector machine," in *2020 IEEE International Conference on Networking, Sensing and Control (ICNSC)*. IEEE, 2020, pp. 1–3.

[30] L. Zheng, H. Cheng, L. Huo, and G. Song, "Monitor concrete moisture level using percussion and machine learning," *Construction and Building Materials*, vol. 229, p. 117077, 2019.

[31] D. Chen, V. Montano, L. Huo, and G. Song, "Depth detection of subsurface voids in concrete-filled steel tubular (CFST) structure using percussion and decision tree," *Measurement*, vol. 163, p. 107869, 2020.

[32] D. Chen, V. Montano, L. Huo, S. Fan, and G. Song, "Detection of subsurface voids in concrete-filled steel tubular (CFST) structure using percussion approach," *Construction and Building Materials*, vol. 262, p. 119761, 2020.

[33] H. Cheng, F. Wang, L. Huo, and G. Song, "Detection of sand deposition in pipeline using percussion, voice recognition, and support vector machine," *Structural Health Monitoring*, vol. 19, no. 6, pp. 2075–2090, 2020.

[34] F. Wang and G. Song, "Looseness detection in cup-lock scaffolds using percussion-based method," *Automation in Construction*, vol. 118, p. 103266, 2020.

[35] F. Wang, G. Song, and Y.-L. Mo, "Shear loading detection of through bolts in bridge structures using a percussion-based one-dimensional memory-augmented convolutional neural network," *Computer-Aided Civil and Infrastructure Engineering*, vol. 36, no. 3, pp. 289–301, 2021. [Online]. Available: https://onlinelibrary.wiley.com/doi/abs/10.1111/mice.12602

[36] K. S. Rao and K. Manjunath, *Speech recognition using articulatory and excitation source features*. Springer, 2017.

[37] J. W. Picone, Ed., *Signal Modeling Techniques in Speech Recognition*, vol. 81, no. 9, 1993.

[38] D. A. Reynolds, "Gaussian mixture models," *Encyclopedia of biometrics*, vol. 741, no. 659-663, 2009.

[39] M. Zhang, X. Chen, and W. Li, "Hidden Markov models for pipeline damage detection using piezoelectric transducers," *Journal of Civil Structural Health Monitoring*, vol. 11, no. 3, pp. 745–755, 2021.